



Kinetic and mechanistic insights into hydrogenolytic production of lignin monomers in a continuous flow-through system

Journal:	<i>Green Chemistry</i>
Manuscript ID	GC-ART-03-2019-000986.R1
Article Type:	Paper
Date Submitted by the Author:	24-Apr-2019
Complete List of Authors:	<p>Li, Yanding; University of Wisconsin Madison, Biological Systems Engineering; University of Wisconsin Madison, DOE Great Lakes Bioenergy Research Center</p> <p>Demir, Benginur; University of Wisconsin Madison, Chemical and Biological Engineering; University of Wisconsin Madison, DOE Great Lakes Bioenergy Research Center</p> <p>Vázquez Ramos, Leida; University of Wisconsin Madison, Chemical and Biological Engineering; University of Wisconsin Madison, DOE Great Lakes Bioenergy Research Center</p> <p>Chen, Mingjie; University of Wisconsin Madison, DOE Great Lakes Bioenergy Research Center</p> <p>Dumesic, James; University of Wisconsin Madison, Chemical and Biological Engineering; University of Wisconsin Madison, DOE Great Lakes Bioenergy Research Center</p> <p>Ralph, John; University of Wisconsin Madison, Biochemistry; University of Wisconsin Madison, Biological Systems Engineering; University of Wisconsin Madison, DOE Great Lakes Bioenergy Research Center</p>

Kinetic and mechanistic insights into hydrogenolysis of lignin to monomers in a continuous flow reactor

Yanding Li,^{†a,b} Benginur Demir,^{†b,c} Leida M. Vázquez Ramos,^{b,c} Mingjie Chen,^b James A. Dumesic^{*b,c} and John Ralph^{*a,b,d}

^aDepartment of Biological Systems Engineering, University of Wisconsin-Madison, Madison, WI 53706, USA.

^bDOE Great Lakes Bioenergy Research Center, University of Wisconsin–Madison, Madison, WI 53706, USA.

^cDepartment of Chemical and Biological Engineering, University of Wisconsin-Madison, Madison, WI 53706, USA.

^dDepartment of Biochemistry, University of Wisconsin-Madison, Madison, WI 53706, USA.

[†]Authors contributed equally to this work.

^{*}Corresponding authors. 3014 Engineering Hall, 1415 Engineering Drive, Madison, WI 53706, USA. Phone: +1 608 262-1095. Fax: +1 608 262-5434. E-mail address: jdumesic@wisc.edu.

2129 WI Energy Institute, 1552 University Ave., Madison, WI 53726-4084, USA. Phone: +1 608 890-2429. E-mail address: jralph@wisc.edu.

Abstract

Industrial biorefineries remain limited due to inefficient valorization of their lignin streams. Rarely can a lignin depolymerization method be combined with a current polysaccharide-centric biorefinery process. Hydrogenolysis is among the more promising methods for depolymerizing lignin on an industrial scale. We performed reaction kinetics and mechanistic studies on lignin model compounds to understand lignin hydrogenolysis pathways, demonstrating that lignin end-units and internal units react significantly differently. Understanding the reaction mechanism and its sensitivity to variables helped us establish a continuous lignin upgrading process from various fractionated lignins. Near-theoretical yields of lignin platform monomers with >80% overall product selectivity were obtained in a continuous hydrogenolysis process using a Pd/C catalyst.

Table of contents entry

Phenolic commodity chemicals were produced from lignin with high yield and selectivity in a flow reactor, valorizing the biorefinery process.

1. Introduction

Environmental issues caused by unrestrained use of fossil energy require a renewable carbon-neutral substitute. Lignocellulosic biomass is one of the most promising alternatives as a widely available sustainable resource. Plant cell wall material typically consists of 40-50% cellulose, 25-30% hemicelluloses, and 15-25% lignin.¹ It can be fractionated into these three component streams, and each stream can be upgraded to fuels and chemicals. However, the recalcitrance of the plant cell wall, lignin in particular, makes biomass fractionation and upgrading inefficient. Most of the current biorefinery processes focus on the conversion of the polysaccharides, in which the biomass fractionation using harsh acids, bases, or additional chemicals, destroys the native lignin structure.²⁻⁴ Under these conditions, lignin undergoes irreversible condensation reactions, such that essentially the only option left for the condensed lignin is to burn it to generate low-value heat.

Due to its aromatic backbone structure and lower oxygen content, lignin has a higher energy density than cellulose and hemicelluloses. A recent energy report claims that at least 50% of the lignin content needs to be utilized to make biorefineries economically viable.⁵ To this end, various lignin deconstruction methods have been developed, such as oxidative/reductive depolymerization, hydrolysis, and biodegradation.²⁻⁴

Native lignin is biosynthesized primarily from its three monolignols: *p*-coumaryl alcohol, coniferyl alcohol, and sinapyl alcohol, via combinatorial radical-coupling reactions.⁶ The most common type of native lignin unit is characterized by its β -O-4 ether interunit linkage (50-60%), and the rest are minor C-C and diaryl ether units.⁷ Full cleavage of the β -ethers therefore leads to effective lignin depolymerization. For this purpose, reductive catalytic fractionation (RCF) of lignin simultaneously fractionates the biomass and cleaves the β -ether linkages.⁸ Lignin hydrogenolysis has been studied since 1938 and, with the evolution of the techniques, high monomer yields with high selectivity can be achieved.⁹⁻¹⁵ There is also a recent study reporting the apparent activation energy of lignin solvolysis and reduction over Ni/C both in batch mode and in flow reactors.¹⁶ However, the reaction kinetics and mechanism of lignin hydrogenolysis are still not well understood for a variety of catalysts and reactor designs.¹⁷ Elucidation of the fundamentals of lignin hydrogenolysis was sought to guide us not only to create active and robust catalysts, but also to model selective reaction environments for the complex upgrading process.

Lignins are often obtained from bulk biomass fractionation processes.^{18,19} Kraft and organosolv lignins are the major technical lignins currently produced on a large scale by the pulp

and paper industry. However, the high sulfur content in the former and the often extremely condensed structure of especially the latter types of lignin make them unsuitable for further upgrading.²⁰ A high-quality lignin stream is essential to add value to the biorefinery process.²¹ Researchers have emphasized the limiting factors towards the lignin depolymerization process, and rationalized a few basic principles of a high-quality lignin ideotype for depolymerization.²² Briefly, when wild-type biomass is used, pretreated lignin with a high β -ether content, such as Cu-AHP lignin, aldehyde-protected lignin, and GVL-lignin, is more valuable for downstream lignin upgrading.²³⁻²⁶

We propose herein a fully continuous biomass refinery as a combination of a traditional biomass pretreatment process with a continuous lignin hydrogenolysis pathway in a flow-through system. We describe a method to obtain value-added platform monomers from the downstream processing of the isolated lignin stream to enhance the biorefinery. With the help of lignin model compounds, the reaction pathways of lignin hydrogenolysis were investigated and a reaction kinetics model was developed. Understanding the reactivity of lignin model compounds helps us design the reaction conditions for actual lignin hydrogenolysis with a Pd/C catalyst.

2. Experimental section

2.1 Compositional analysis

Klason lignin and monosaccharides analysis was performed by the two-stage sulfuric acid hydrolysis following the optimized NREL standard protocol (Table S2).^{22,27}

2.2 Lignin isolation

Poplar wood chips, without prior solvent extraction, with a Klason lignin content of 19.1 ± 1.0 wt% were ground on a Wiley mill to pass through a 1 mm screen. *Mild-acidolysis lignin*: Poplar 10 g (dried weight) was suspended in 120 mL of dioxane/water mixture (9:1, v/v) containing 0.2 mol/L HCl in a 1 L round-bottom flask. The suspension was refluxed in a pre-heated oil bath at 120 °C for 1.5 h. The suspension was cooled, filtered through a Büchner funnel. The solution was neutralized by adding saturated NaHCO₃ solution until pH ~4. Then the solution was concentrated to about 50 mL under vacuum at 50 °C. Lignin was precipitated by pouring the concentrated solution into 500 mL ice-water. The precipitated lignin was collected by centrifugation and washed with water (3 times) and then freeze dried. Mild-acidolysis lignin yield (on a Klason lignin basis):

94.2%. *GVL lignin* was prepared as previously described.²⁶ *Cu-AHP lignin* was prepared as previously described.²³

2.3 Catalytic activity measurements in a flow-through reactor

Hydrogenolysis of lignin and lignin model compounds was carried out in a flow-through system as illustrated in Fig. S1. The designated amount of catalyst was mixed with α -Al₂O₃ (α -Al₂O₃: Pd/C = 10:1) and loaded on top of a bed containing silica chips in a 0.25" i.d. stainless steel tubular reactor. The catalyst was immobilized by placing quartz wool at the top and the bottom of the catalyst bed as well as the bed of silica chips (mesh 24). The system was pressurized with argon or hydrogen to 500-900 psi. The fixed bed reactor in an up-flow configuration was placed in an aluminum block and heated to the reaction temperature (100-200 °C) under H₂ flow 20 cm³ (STP)/min using an insulated furnace. Temperature was measured by a K-type thermocouple (Omega) at the reactor wall and controlled by programmable temperature controller (16A series, Love Controls). In a typical experiment, 0.05 g of Pd/C (Aldrich) was packed with 0.5 g α -Al₂O₃. Reaction kinetics parameters were obtained by flowing gas [20 cm³ (STP)/min, H₂ or Ar] and by introducing model compound/lignin solutions (1-4 mg/mL) in methanol with 0.2 mL (STP)/min flow rate using an HPLC pump (Lab Alliance Series I) at 100-140 °C and 500-900 psi gas pressure. The homolysis of lignin model compounds at 200 °C was achieved using γ -valerolactone (GVL) as a solvent at 800 psi Ar with 0.2 mL/min of feed solution (2 mg/mL **GG** / **VG** in GVL), 20 mL/min Ar.

For the lignin hydrogenolysis reaction, the feed solution was prepared by dissolving the lignins in dioxane/water (9:1, v/v) at room temperature. The solution was sonicated before using in the flow-through system. Fresh catalyst was used for the dissolved lignin experiments.

2.4 Lignin hydrogenolysis in a Parr batch reactor

Isolated lignin (100 mg) was dissolved in 30 mL dioxane/water (9:1, v/v) and transferred into a 50-mL high-pressure Parr reactor along with 50 mg of catalyst (5 wt% Pd/C). The reactor was stirred with a mechanical propeller and heated via a high-temperature heating jacket. Once closed, the reactor was purged three times and then pressurized with H₂ (30 bar). The reactor was heated to 200 °C in 15 min and then held at 200 °C for 3 h. After the reaction was complete, the reactor was cooled to room temperature. The resulting liquid was filtered through Celite and washed with

EtOH. The solvent was removed under reduced pressure at 40 °C with a rotary evaporator. The crude products were dissolved in EtOH and made up to 10 mL in a volumetric flask. A 1 mL aliquot was transferred into three 5-mL vials and then dried under reduced pressure. The dried samples were used for GC, GPC, and NMR analysis.

GC sample preparation: The sample solution in EtOH was diluted 10 times with EtOH and then analyzed by GC-FID. GPC sample preparation: The sample solution was diluted 10 times with DMF and filter through a 0.2-micron PTFE membrane filter and then analyzed by GPC.

NMR sample preparation: The sample solution was dried *in vacuo*, then dissolved in 0.6 mL DMSO-*d*₆/pyridine-*d*₅ (4:1, v/v) and transferred to a 5 mm NMR tube for NMR.

2.5 Quantitative HPLC analysis of reaction products from lignin model compounds

Samples collected from the flow-through reactor were filtered through a 0.2 μm PTFE membrane filter before injected to the HPLC. The concentrations of the samples were determined by HPLC using a WATERS 2695 separations module with a WATERS 2998 PDA detector set at 275 nm. The analytical HPLC column set consists of a Luna C18 (Phenomenex) HPLC column and a guard column [guard column → Luna C18 4.6 mm inner diameter (ID) × 250 mm and 5 μm particle size]. The column oven was held at 50 °C during analysis. The mobile phase was a gradient acetonitrile/water (with 0.1% formic acid) at 1.0 mL/min flow rate. HPLC data were processed by EMPOWER2 postrun software. External calibrations with authentic standards were used to quantify the concentrations of reactants and products. Yield of β-ether cleavage was calculated as follows.

$$\text{Conversion (\%)} = \frac{[\text{Reactant}]^o - [\text{Reactant}]}{[\text{Reactant}]^o} \times 100 \quad (1)$$

$$\beta - \text{ether cleavage (\%)} = \frac{[\text{Guaiacol}]}{[\text{Reactant}]^o} \times 100 \quad (2)$$

$$\text{Product Yield (\%)} = \frac{[\text{Product}]}{[\text{Reactant}]^o} \times 100 \quad (3)$$

Where,

$[\text{Reactant}]^o$ is the initial concentration of reactant in the feed;

$[\text{Guaiacol}]$ and $[\text{Product}]$ are the concentrations of guaiacol and other products in the effluent, respectively.

2.6 Catalyst characterization

CO chemisorption at 24 °C was used to determine palladium surface site density of the fresh Pd/C catalyst. CO adsorption/desorption isotherms were measured (Fig. S2), the active Pd site density was found 55 μmol/g and the Pd dispersion was calculated as 12%. Using this site density of the catalyst, the turnover frequency (TOF) for product formation was calculated as shown in Eqn 5.

2.7 Reaction rate calculation

$$rate = \frac{([Guaiacol] - [Guaiacol]^o) \times flow\ rate}{catalyst\ weight} \quad (4)$$

$$TOF = \frac{rate}{site\ density} \quad (5)$$

$$rate_{GG} = k_{GG} [GG]^m \left[\frac{P_{H_2}}{H} \right]^n \quad (6)$$

$$rate_{VG} = k_{VG} [VG]^m \left[\frac{P_{H_2}}{H} \right]^n \quad (7)$$

$$k = Ae^{-\frac{E_a}{RT}} \quad (8)$$

Where,

$[Guaiacol]^o$ is the initial concentration of guaiacol;

$[Guaiacol]$, $[GG]$, $[VG]$, $[P_{H_2}/H]$ are the concentration of guaiacol, GG , VG , and H_2 ;

H is the Henry's law constant;

m is the reaction order for model compounds;

n is the reaction order for H_2 ;

A is the pre-exponential factor;

E_a is the activation energy.

2.8 NMR spectroscopy

NMR spectra were acquired on a Bruker Biospin AVANCE-III 700 MHz spectrometer fitted with a cryogenically-cooled 5-mm QCI $^1H/^{31}P/^{13}C/^{15}N$ gradient probe with inverse geometry (proton

coils closest to the sample), and spectral processing was performed using Bruker's Topspin 4.0.4 (Mac) software. For NMR experiments, lignins were dissolved in DMSO- d_6 /pyridine- d_5 , model compounds, HPLC fractionated compounds, and hydrogenolysis products mixture from lignins were dissolved in acetone- d_6 . The central solvent peaks were used as the internal references (δ_C/δ_H : DMSO, 39.5/2.49; acetone, 29.84/2.05 ppm). Standard Bruker implementations of the traditional suite of one-dimensional (1D) and two-dimensional (2D) [gradient-selected, ^1H -detected; for example, correlation spectroscopy (COSY), ^1H - ^{13}C heteronuclear single-quantum coherence (HSQC), and heteronuclear multiple-bond correlation (HMBC)] NMR experiments were used for structural elucidation and assignment authentication. HSQC processing used typical matched Gaussian apodization in F2 (LB = $-0.5 \text{ GB} = 0.001$) and squared cosine-bell apodization in F1.

2.9 GC-MS qualitative analysis of low molecular weight products

Samples were dissolved in pyridine and BSTFA (*N,O*-bis(trimethylsilyl)trifluoroacetamide) was added for TMS derivatization. The mixture was heated to 50 °C for 30 min. An aliquot of the sample (1 μL) was injected by an autosampler into a GC-MS (Shimadzu GC2010/PARVUM2, IC-1 column) equipped with a fused-silica capillary column (15 m \times 0.25 μm film, Zebron ZB-5HT Inferno capillary column, Phenomenex Co.) operating in split mode (split ratio 20:1) to identify the products. The products were identified by comparison with the peak retention times and mass spectra of the authentic compounds and (or) by comparing with entries in the National Institute of Standards and Technology (NIST) mass spectral library.

2.10 GC-FID quantitative analysis of low molecular weight products from lignin hydrogenolysis

The samples were collected from the flow reactor and injected without derivatization. An aliquot of the sample (1 μL) was injected by an autosampler into a GC-FID (Shimadzu GC2014) equipped with a fused-silica capillary column (15 m \times 0.25 μm film, Zebron ZB-5HT Inferno capillary column, Phenomenex Co.) operating in split mode (split ratio 20:1) to quantify the products. The identified major products were quantified using external calibration curves derived from authentic synthetic compounds. The products were identified by comparison with the peak retention times.

2.11 NMR quantification and theoretical monomer yield calculation

The NMR resolved lignin linkages can be calculated based on the integrals of α - $^1\text{H}/^{13}\text{C}$ correlation peaks versus the integrals of the aromatic- $^1\text{H}/^{13}\text{C}$ correlation peaks in the HSQC spectra as follows:

$$A\% = \frac{I_A}{0.5(I_{S_{2,6}} + I_{S'_{2,6}} + I_{S_{condensed}}) + I_{G_2}} \times 100 \quad (9)$$

$$B\% = \frac{I_B}{0.5(I_{S_{2,6}} + I_{S'_{2,6}} + I_{S_{condensed}}) + I_{G_2}} \times 100 \quad (10)$$

$$C\% = \frac{0.5I_C}{0.5(I_{S_{2,6}} + I_{S'_{2,6}} + I_{S_{condensed}}) + I_{G_2}} \times 100 \quad (11)$$

Where,

A is the integral of the α -C/H correlation peaks from the β -O-4 units;

B is the integral of the α -C/H correlation peaks from the β -5 units;

C is the integral of the α -C/H correlation peaks from the β - β units;

$S_{2,6}$ is the integral of the 2/6 correlation peaks from the syringyl aromatic ring;

$S'_{2,6}$ is the integral of the 2/6 correlation peaks from the benzyl-oxidized syringyl aromatic ring;

$S_{condensed}$ is the integral of the 2/6 peaks from the condensed syringyl aromatic ring;

G_2 is the integral of the correlation from the 2-position of the guaiacyl aromatic ring;

From the equations above, the contents of the resolved lignin linkages by HSQC NMR are listed, and the theoretical monomer yield²⁸⁻³⁰ can be calculated using Eqn. 12:

$$Y = \frac{(n-2)P^2 + 2P}{n} \times KL \times 100 \quad (12)$$

Where,

Y is the summation of the monomer aromatics;

n is the number of monomers occurring in the lignin polymer;

P is the fraction of cleavable/targeted bonds, in this case, the β -O-4 bond;

KL is the Klason lignin content (Table S2);

In the case of the hydrogenolysis reaction, the lignin end-units (**CA**, and **SA**) can be converted to the target monomers (**DCA** and **DSA**). Thus, Eqn. 12 can be simplified to Eqn. 13:

$$Y \approx P^2 \times KL \times 100 \quad (13)$$

The NMR integrals and theoretical monomer yields are listed in Table S3.

2.12 Gel-permeation chromatography (GPC)

Molecular weight distributions of lignin were determined by GPC using a Shimadzu LC20-AD LC pump equipped with a Shimadzu SPD-M20A UV detector set at 280 nm and a Polymer Standard Services GPC column and guard column [PSS PolarSil analytical Linear S, 8-mm inner diameter (ID) \times 5 cm and 5-mm particle size \rightarrow PSS PolarSil analytical Linear S, 8-mm ID \times 30 cm and 5-mm particle size]. The column oven was held at 50 °C during analysis. The mobile phase was DMF, and the flow rate was 0.3 mL/min. Molecular weight distributions were determined using Shimadzu GPC post-run software via a conventional calibration curve using a ReadyCal polystyrene Kit from Sigma-Aldrich [Aldrich # 76552, M(p) 250-70000]. The molecular weight distributions of the depolymerization products were determined using a series of synthetic standard compounds (Fig. S37).

2.13 Synthetic model compounds

Synthetic methods are described in the SI.

2.14 Liquid/gas phase simulation

Aspen simulations of the liquid fraction of the reaction solvents in the reaction media are described in the SI (Fig. S3-S5).

3. Results and discussion

3.1 Model compound study, and kinetic modeling

Two all-guaiacyl β -ether lignin model compounds, guaiacylglycerol- β -guaiacyl ether (**GG**) and veratrylglycerol- β -guaiacyl ether (**VG**), were used to model the phenolic end-units and internal units of the lignin polymer, respectively (Scheme 1). It is crucial to use realistic lignin model compounds because every aspect of the structure, as found in real lignin, significantly affects the reactivity.³¹⁻³⁸ The hydrogenolysis reactions of model compounds were performed in the flow-

through reactor (Fig. S1), which is an effective system to explore lignin reaction mechanisms and kinetics.³⁹⁻⁴²

The reaction kinetic parameters for lignin model compounds over 5 wt% Pd/C were determined within the kinetically controlled regime by keeping the extent of β -ether cleavage below 25%. The compounds were dissolved in methanol at various concentrations (1-4 mg/mL) and continuously fed to the flow-through reactor at a range of temperatures (100-200 °C) and pressures (500-900 psi). Aspen simulations confirmed that the solvent remains in its liquid phase under these conditions (Fig. S3-S5). The overall mass balance around the flow system was conserved for all the reactions reported in this study, as demonstrated in Table S8. Accordingly, reaction rate constant (k), reactant order (m), H_2 order (n), and activation energy (E_a), were calculated by equations 4-10 as given in the methods section.

The phenolic model compound **GG** underwent homolysis without any catalyst (Scheme 1, pathway a-II) under neutral conditions (i.e., no acidic or alkaline additives), producing coniferyl alcohol (**CA**) as the main product (Fig. S6). The HPLC chromatograph (Fig. S8a) demonstrated that homolysis products such as **G** and **CA** from **GG** were detected at 160 °C and at 200 °C. The product selectivity for guaiacol (**G**), 45%, was higher than the **CA** selectivity, 20% at 200 °C. The discrepancy between the product selectivities is due to the rapid condensation/degradation of **CA**. The β -ether cleavage was accomplished in a short reaction time (residence time of 15 mins) using the flow-through reactor. The analogous reaction was not observed for the etherified model compound **VG** (Scheme 1, pathway b-II), even at the increased temperature of 200 °C (Fig. S7). The homolysis products from **VG** homolysis at 200 °C, guaiacol (**G**) and veratryl alcohol (**VA**), were not detected by HPLC (Fig. S8b). These results are consistent with previous studies using model compounds, suggesting that lignin homolysis only occurs from the end-units through a quinone methide intermediate.^{43,44} Peeling of end-groups from lignin structure in the flow system has been proposed previously; however, these studies focused on the pulping process, not the hydrogenolysis reaction. The peeling mechanism during lignin hydrogenolysis remains obscure. For instance, Samec et al. discussed Pd-free depolymerization of lignin (i.e., the organosolv pulping mechanism) under acidic conditions.⁴¹

The hydrogenolysis of **GG** and **VG** over Pd/C catalyst resulted in dihydroconiferyl alcohol (**DCA**) and dihydroveratryl alcohol (**DVA**) with >90% selectivity (Fig. S9-17, S20-27) (Scheme 1, pathways a-I and b-I). The **GG** hydrogenolysis was approximately 2.3 times faster than that of

the **VG** reaction (Table 1). This result indicates that a peeling reaction pathway from the polymer's phenolic end-units is much faster for lignin hydrogenolysis. The reaction orders for the reactants (*m*) and hydrogen (*n*) are similar (Fig. 1a-b, Table 1) for both model compounds. In addition, the activation energies ($E_{a_{H_2}}$) for hydrogenolysis are not significantly different: 72 kJ/mol for **GG** and 78 kJ/mol for **VG** (Fig. 1c, Table 1). The homolysis activation energy ($E_{a_{hom}}$) was reported in the literature as 98 kJ/mol, implying that the Pd/C catalyst lowers the energy barrier for β -ether cleavage by 26 kJ/mol.⁴⁵ The hydrogenolysis of β -ether units may not favor a quinone methide pathway (Scheme I, pathway a-II and b-II), as the low activation energy routes (Scheme I, pathway a-I and b-I) are more favorable.

Under argon (Ar) flow (Fig. S18-19, S28), Pd/C catalyzed unwanted reactions such as the formation of isoeugenol (**IE**) together with a significant amount of the side-chain-truncated products, such as ethyl guaiacol (**EG**) (Scheme 1, pathway a-V and b-V). The activation energy values ($E_{a_{Ar}}$) for the reactions of **GG** and **VG** under Ar flow are comparable (Fig. 1d). However, when the reactivity of the hydrogenolysis reaction and that of the catalytic reaction under Ar are compared for both model compounds (Table 1), the hydrogenolysis reaction (under H_2) is approximately 4 times faster than the reaction under Ar. Also, the value of $E_{a_{H_2}}$ (70 kJ/mol) is much lower than the value of $E_{a_{Ar}}$ (120 kJ/mol). The implication is that, when the reaction medium is saturated with H_2 , the reaction proceeds through the hydrogenolysis pathway (Scheme 1, pathway a-I and b-I), and the production of undesired compounds can be suppressed. In the absence of H_2 , **GG** can react to give either **CA** or the aforementioned undesired compounds (Scheme I, pathway a-II and a-V).

CA in methanol was fed to the reactor under H_2 and Ar to study whether the hydrogenolysis reaction of **GG** could proceed through the intermediate **CA**, even though it is not favorable (pathway a-III and a-IV corresponding to the reaction under H_2 and Ar, respectively), in addition to the direct conversion route (pathway a-I and a-V reactions under H_2 and Ar, respectively). The products obtained from these experiments were analogous to those obtained from the **GG** reaction, but with a much faster reaction rate (Fig. S29-30). That is, if the homolysis of **GG** occurs, **CA** will readily convert to its corresponding stabilized products over the catalyst.

We conclude that lignin model compounds follow different reaction pathways depending on the temperature and the presence of H_2 . Herein, we established the reaction pathways and developed the corresponding reaction kinetics model by carrying out the reactions to elucidate the

significance of each step on the free-phenolic model **GG** (representing lignin phenolic end-units) and the etherified model **VG** (representing lignin internal units). Understanding the reaction kinetic model and the mechanism allowed us to achieve high yield and selectivity of desired products under certain reaction conditions. For instance, increasing the reactant concentration should enhance the hydrogenolysis rate, as shown by the positive order with respect to the reactant (m). The reaction order of H_2 (n) is lower than the reaction order of reactant (m), indicating that excess H_2 is not necessary as long as there is sufficient H_2 mass transfer between the gas and liquid phases. The $E_{a_{H_2}}$ of pathway a-I and b-I is much lower than the $E_{a_{Ar}}$ of pathway a-V and b-V, illustrating that mild temperatures should be applied at short reaction times to avoid the unwanted side-reactions. Therefore, the yield and selectivity of the target products (i.e., **DCA** and **DVA**) can be maximized.

3.2 Lignin hydrogenolysis in a flow-through reactor

Based on the results of our studies of model compounds, the complete cleavage of β -ethers in lignin should be achieved under the appropriate reaction conditions (i.e., reactant concentration, H_2 pressure, and temperature). Moreover, the kinetic model predicted a faster reaction rate for the phenolic end-units of lignin polymer compared to the internal units. Accordingly, at mild temperatures (<140 °C), a lignin polymer can be shortened by peeling reactions from the phenolic end while maintaining some β -ether linkages in the interior of the polymer chain. At elevated temperatures, these internal linkages are also cleaved, allowing the maximal yield of lignin monomers to be achieved.

To probe the aforementioned predictions of our reaction kinetics studies, three lignin isolates (Cu-AHP lignin, mild-acidolysis lignin, and GVL-lignin) produced from poplar were studied under the same conditions in the flow-through reactor. Here, the data from Cu-AHP lignin are discussed as an example; results from the hydrogenolysis of mild-acidolysis and GVL lignins are summarized in Table S4-6, and Fig. S33-36.

The isolated lignin cannot be dissolved in methanol but can be readily solubilized in dioxane/water (9:1, v/v) at room temperature. To justify the kinetic models established in MeOH, we also measured the reaction rate and activation energy of the model compound **GG** in dioxane/water (Fig. S31-32). The β -ether cleavage reaction rate in dioxane/water was lower than

that obtained in methanol, but the product distribution did not differ significantly when the solvent was changed.

We carried out **GG** and **VG** hydrogenolysis reactions at high temperature (190 °C) as shown in Fig. 2. The products obtained in **GG** hydrogenolysis in methanol (Fig. 2a-2) were the same as those observed at lower temperature. In dioxane/water, the product distribution was slightly altered at 190 °C (Fig. 2a-3). Although some side-reactions were detected, the major products remained the same at low temperature both in methanol and in dioxane/water. The products obtained in **VG** hydrogenolysis both in methanol (Fig. 2b-2) and in dioxane/water (Fig. 2b-3) remained the same when we compared these results with the reactions at lower temperatures. The reaction rate in dioxane/water was lower than that in methanol as we observed in **GG** hydrogenolysis. This behavior could explain the observation that the yield of hydrogenolysis products of lignin in dioxane was lower than that in MeOH, as previously reported.⁴⁶

The reason for the carbon loss in the hydrogenolysis reaction at high temperature is due to the production of partially ring-saturated compounds, as detected in the high-resolution mass spectrum. These products were produced from the ring-saturation of one or both of the aromatic rings of the **GG** and **VG** models. We could not quantify these products due to the lack of proper model compounds. Thus, the carbon balance at 190 °C was lower compared to the carbon balance at low temperatures. The study carried out with model compounds in methanol was useful to understand the hydrogenolysis of biomass-derived lignin in the dioxane/water mixture.

The lignin soluble in dioxane/water behaved similarly to the lignin model compounds under hydrogenolysis conditions from 140 °C to 190 °C. The monomer yields and product distribution as a function of time were analyzed using GC-FID (Fig. 3a-b). The main products of lignin hydrogenolysis were **DCA/DSA**, consistent with our model compound study. The yield for the monomers increased with increasing temperature (Fig. 3b), and the monomer yields at 190 °C were similar to those obtained from a batch reaction (Fig. 3a). During the reaction period (10 h), neither catalyst deactivation nor gas products were observed under the current reaction conditions. The Cu-AHP lignin solution showed a peak in the high molecular weight region of its GPC chromatogram due to the aggregation of lignin polymers in the dioxane/water solution (Fig. 3c). Monomer production was observed at 140 °C mainly because of the fast reaction rate of the lignin end-units. Low molecular weight fractions increased and high molecular weight fractions decreased with elevated reaction temperatures. Although no significant accumulation of

monomers at 140 °C was observed, there was a sharp decrease of the aggregated lignin peak. This decrease was mainly due to the hydrodeoxygenation of the hydroxyl groups in the lignin that disrupts hydrogen bonds. As the temperature was changed from 140 °C to 190 °C, the molecular weight was reduced because of the cleavage of both lignin end-units and internal units. Finally, at 190 °C, the product molecular weight distribution was the same as that of the batch reaction, with the highest molecular weight product at a tetramer level (~800 Da), as has been observed in other reactions in which β -ether units are fully cleaved.⁴⁷

The 2D HSQC NMR spectra illustrate that the major lignin sidechain units (β -O-4, β -5, and β - β) in the Cu-AHP lignin were well resolved in the sidechain fingerprint region (Fig. 4a). The aromatic signals were similar to those from native lignin, apart from a small amount of the benzylic oxidation caused by the Cu-AHP pretreatment method.²³ The signals of the lignin sidechain units showed no obvious changes before and after the reaction, at 140 °C and 160 °C. In the aromatic region, two new **S'** peaks appeared (δ_C/δ_H : 106.1/6.48, and 107.3/6.65 ppm) at slightly higher magnetic field from the original **S** peak (δ_C/δ_H : 104.7/6.78 ppm). The **S'** peaks were assigned to the corresponding aromatic groups of the α -alkyl type syringyl-units, which derived from the hydrodeoxygenation of the original α -benzylic hydroxy group in the lignin. Similarly, the **G'** peaks (δ_C/δ_H : 113.0/6.77, and 120.8/6.60 ppm) were assigned to the α -alkyl type guaiacyl-units. **S'** and **G'** peaks are present in either the hydrogenolysis monomers (**DCA** and **DSA**) or the α -alkyl type lignin oligomers (Table S7). No **S'** and **G'** were present in the Cu-AHP lignin, so those peaks arose because of the hydrodeoxygenation reaction. The ratio of **S** to **S'** was 69:31 and **G** to **G'** was 46:54 at 140 °C. As the temperature increased to 160 °C, the ratio of **S** to **S'** decreased to 46:54, and **G** to **G'** decreased to 15:85. At 190 °C, the ratio of **S** to **S'** further decreased to 5:95, and the **G** was quantitatively converted to **G'**. The degree of lignin depolymerization was clearly related to the relative ratio of the native lignin aromatic peaks (**S** or **G**) to the α -alkyl type aromatic peaks (**S'** or **G'**) in 2D HSQC NMR, which correlated well with the GPC analysis. It suggests that, at 190 °C, there was neither β -ether lignin units nor remaining high molecular weight lignin polymers, meaning that almost all of the β -ether bonds were cleaved under this reaction condition. We also concluded that the unreacted lignin demonstrated no apparent structural change during the hydrogenolysis reaction. Thus, the product stream can be recycled to accomplish higher yields at moderate temperatures (<190 °C) without the loss of carbon to undesirable condensation reactions.

A significant number of unidentified peaks appeared in the oxygenated aliphatic fingerprint region of the HSQC NMR (Fig. 4b-d). We hypothesize that these peaks came from the reactions of polysaccharides which, compositional analysis showed, were still present in substantial amounts in the isolated lignins (Table S2). Under these conditions, polysaccharides undergo ring-opening, dehydration, and hydrogenolysis, creating polyols for which peaks appear in the oxygenated aliphatic region.^{48,49}

Although no β -ether bonds remained after the 190 °C reaction according to the HSQC NMR and the GPC analysis, a monomer yield of 100% can not be expected. Unlike in the model compounds, other non-cleavable units are present in real lignin, which can also suffer structural changes during isolation. The theoretical lignin monomer yield, Y , can be estimated from Eqn. 13. The relative β -ether percentage content in the Cu-AHP lignin was 61.6% as estimated by HSQC NMR (Table S3). Thus, after the compositional analysis correction for lignin content, the theoretical lignin monomer yield of the Cu-AHP lignin was calculated as 31.2% (Table S3). The monomer yields obtained in the continuous flow reaction at 190 °C (28.4%) as well as the batch reaction (29.0%) are thus near the theoretical limit. Full cleavage of the β -ether bonds can therefore be accomplished in a continuous-flow reactor. As the lignin monomers can be produced at large scale, a following separation step such as vacuum or steam distillation can be applied, providing a new aspect for economical process optimization of lignin valorization.

4. Conclusions

In this study, two lignin model compounds were used to study lignin hydrogenolysis reaction pathways and mechanisms. Applying the information we collected from studies of model compounds, a continuous lignin upgrading process was established using soluble lignin in a flow-reactor. The advantages of the flow-through system include the continuous production of lignin monomers at high yield and selectivity by optimizing reaction parameters such as reaction temperature, pressure, and flow-rate in real time. The new lignin upgrading system can be combined with traditional biomass pretreatment methods to enhance the yield and value of phenolic commodity chemicals that valorize the overall biorefinery process.

Online Content

Additional Methods, Extended Data, and Source Data are available in the online version of the paper; references unique to these sections appear only in the online paper.

Supplementary Information is available in the online version of the paper.

Acknowledgements

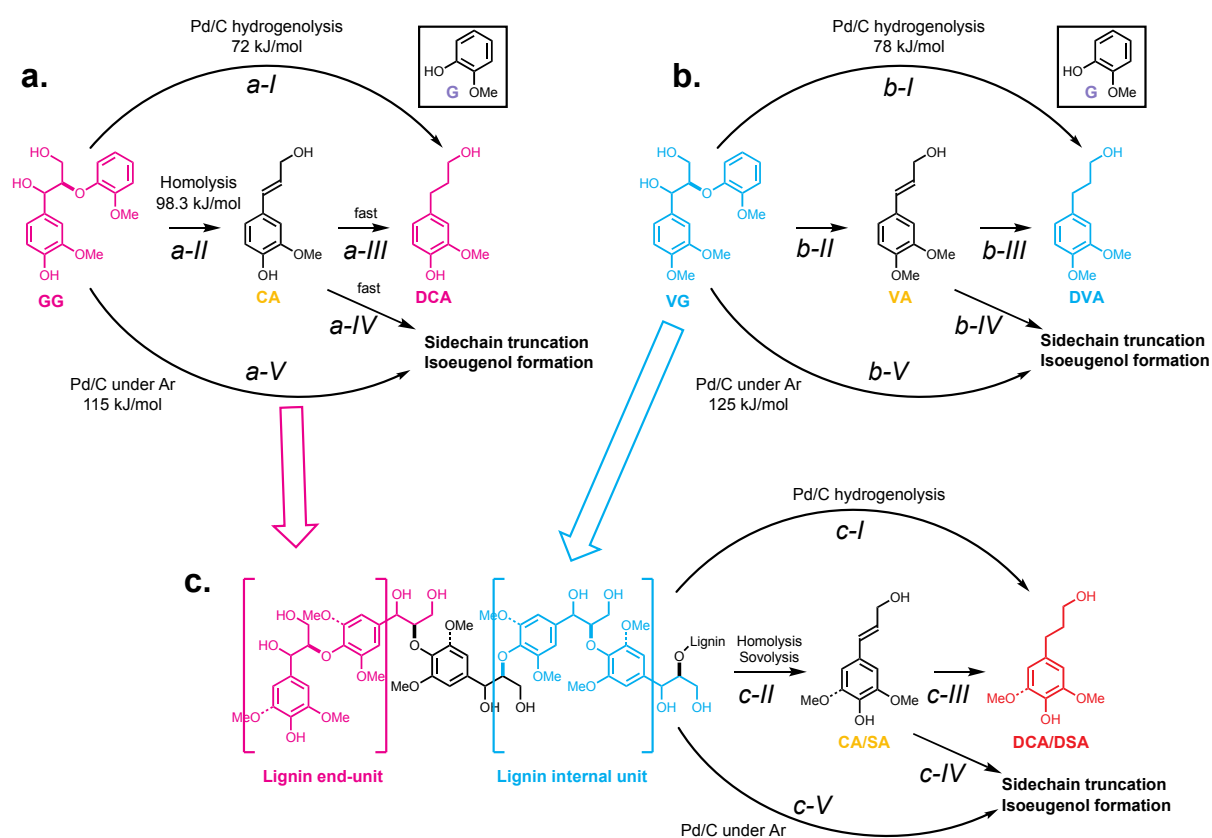
Funding was provided by the DOE Great Lakes Bioenergy Research Center (DOE BER Office of Science DE-SC0018409). We are grateful to Dr. Ning Li and Prof. Xuejun Pan (U. Wisconsin-Madison) for help with compositional analysis. We are also grateful to Dr. Eric Hegg (Michigan State University, GLBRC) for providing Cu-AHP lignin samples.

Author Contributions

Y.L., B.D., J.R., and J.A.D. were responsible for the conception, planning, and organization of experiments. Y.L. performed the synthesis and characterization of model compounds. B.D. performed the phase simulation in Aspen and catalyst characterization. Y.L., B.D. and L.M.V.R. performed the hydrogenolysis experiments, quantified, and identified the products. Y.L. and B.D. established the kinetic model and reaction pathway. M.C. performed the compositional analysis and lignin isolation. Figures were prepared by Y.L. and B.D., L.M.V.R. aided the experimental design and manuscript writing. The manuscript was primarily written by Y.L., B.D., J.R. and J.A.D. with critical input from all coauthors.

Author Information

The authors declare no competing financial interests. Readers are welcome to comment on the online version of the paper. Correspondence and requests for materials should be addressed to J.R. (jralph@wisc.edu) and J.A.D (jdumesic@wisc.edu).



Scheme 1. Proposed reaction mechanism for hydrogenolysis. a) GG model compound hydrogenolysis, modeling phenolic end-units; b) VG model compound hydrogenolysis, modeling etherified internal units; c) Lignin hydrogenolysis.

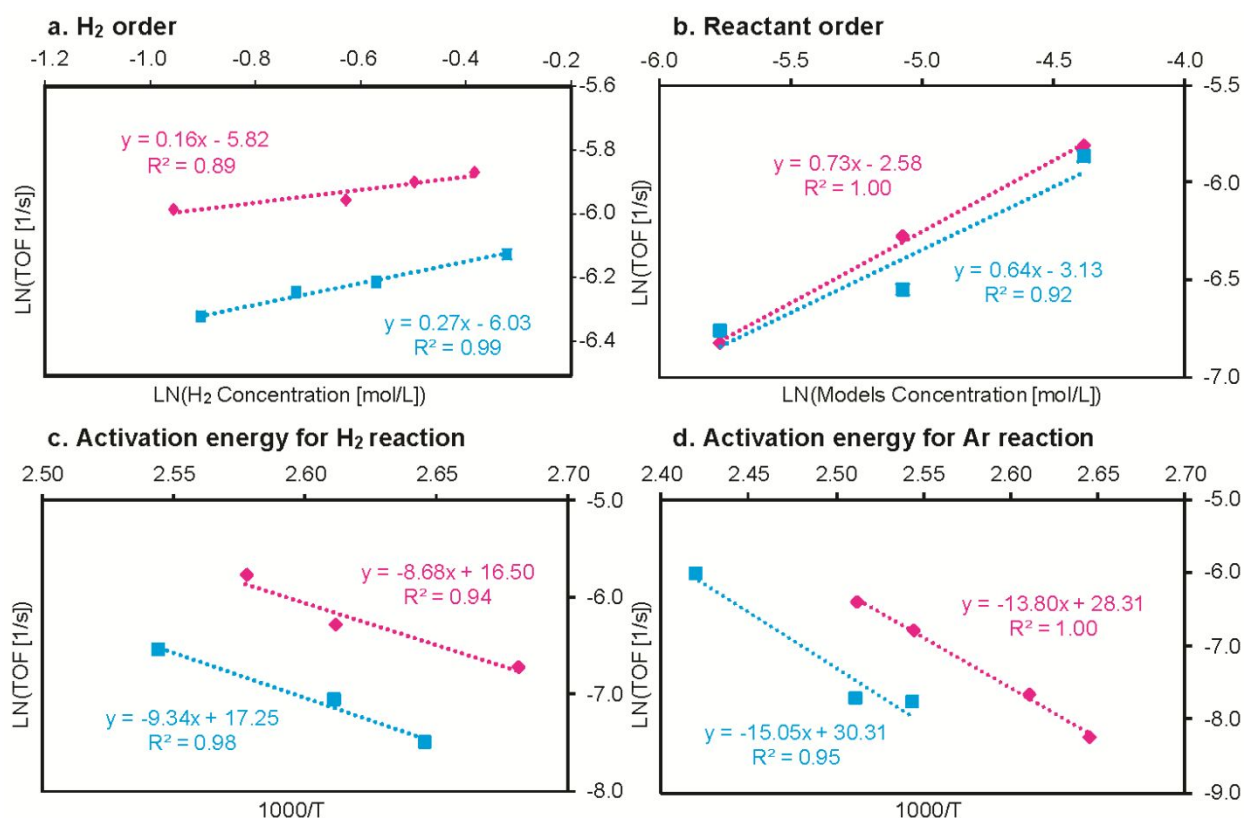


Figure 1. Reaction rate parameters for GG (magenta diamond) and VG (cyan rectangle) model compounds; a) The effect of hydrogen partial pressure on the turnover frequency of hydrogenolysis at 110 °C for **GG** (see also Fig. S15-S17) and at 120 °C for **VG** (Fig. S26-S27). Hydrogen partial pressure varied from 500 to 900 psi. Henry's law constant for hydrogen solubility in methanol is 7.60E-04 M/psi at 110 °C and 8.08E-04 M/psi at 120 °C;⁵⁰ **b)** The effect of model compound concentration on the turnover frequency of hydrogenolysis at 110 °C for **GG** (Fig. S13-S14) and at 120 °C for **VG** (Fig. S24-S25). Model compound concentration varied from 1 to 4 mg/mL; **c)** Arrhenius plot for model compound hydrogenolysis from 100 °C to 115 °C for **GG** (Fig. S10-S12) and from 105 °C to 120 °C for **VG** (Fig. S21-S23) under 20 mL/min H₂ flow, 50 mg 5 wt% Pd/C; **d)** Arrhenius plot for model compound catalytic reaction in Ar from 105 °C to 125 °C for **GG** (Fig. S18-S19) and from 120 °C to 140 °C for **VG** (Fig. S28) under 20 mL/min Ar flow, 50 mg, 5 wt% Pd/C.

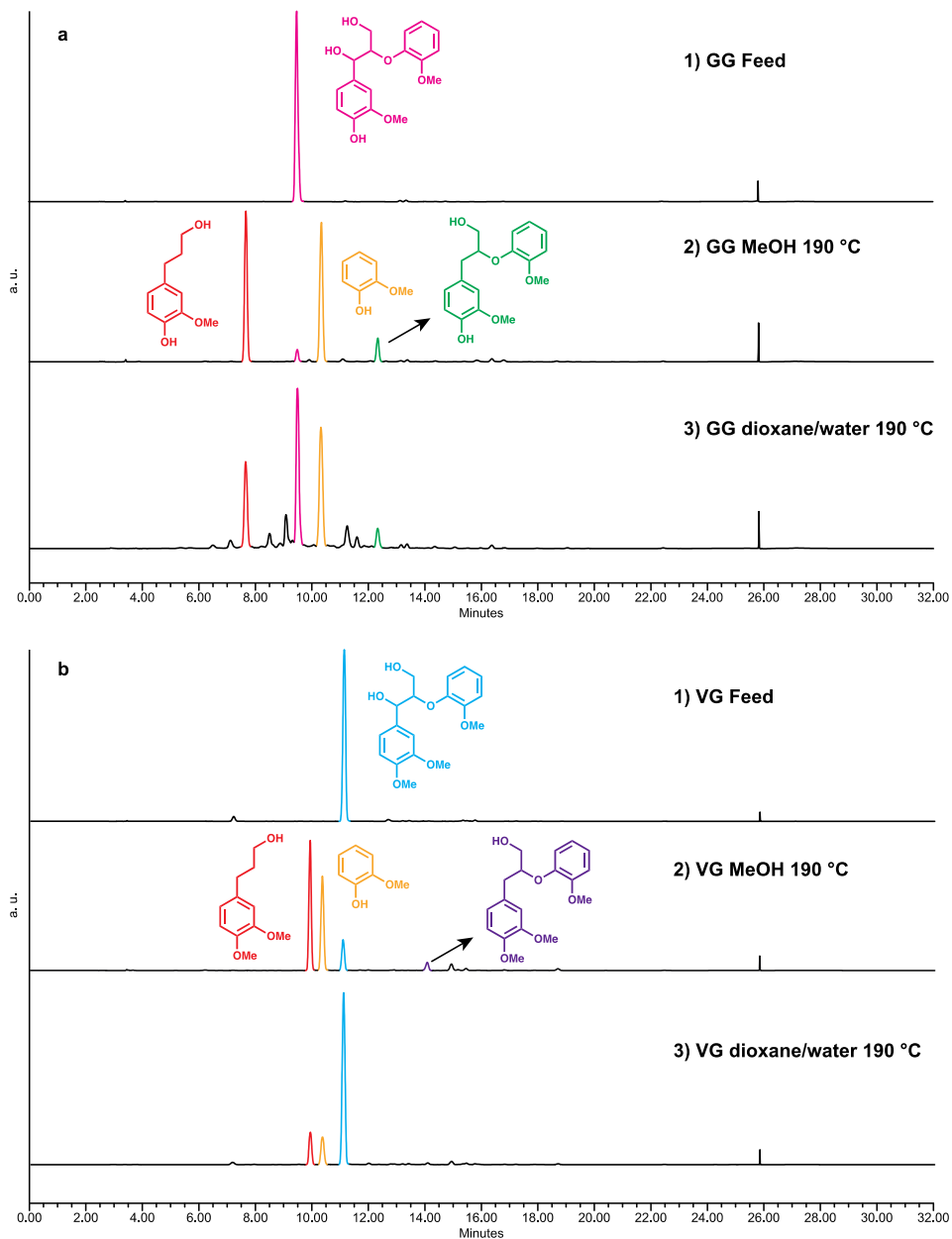


Figure 2. The HPLC chromatograph of the hydrogenolysis reaction of GG (a) and VG (b) at 190 °C. a-1) GG feed; a-2) Products distribution in MeOH; a-3) Product distribution in dioxane/water (9:1, v/v); b-1) VG feed; b-2) Product distribution in MeOH; b-3) Product distribution in dioxane/water (9:1, v/v). The intermediate compounds were confirmed by high-resolution mass spectrometry. The intermediate from the GG reaction, colored green, had HR-MS (ESI) calculated for $C_{17}H_{21}O_5$ $[M+H]^+$: 305.1380; found: 305.1384. The intermediate, colored purple, from the VG reaction, had HR-MS (ESI) calculated for $C_{18}H_{23}O_5$ $[M+H]^+$: 319.1542; found: 319.1540.

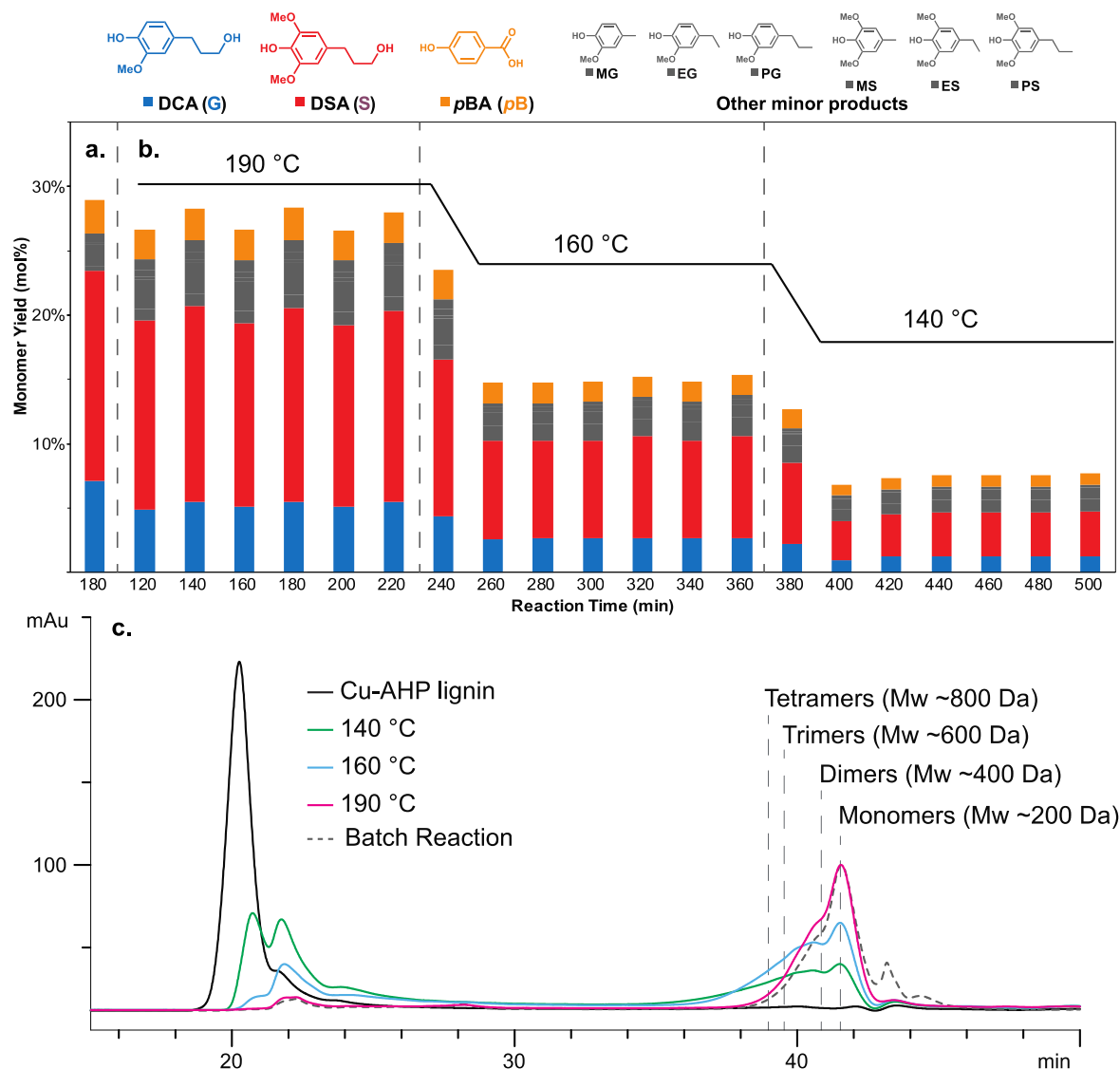


Figure 3. Monomer yields for lignin hydrogenolysis. **a)** The Cu-AHP lignin hydrogenolysis products in the batch reactor: 100 mg Cu-AHP lignin, 30 mL dioxane/water (9:1, v/v), 50 mg 5% Pd/C, 3 h, 450 psi H₂ (STP), 200 °C; **b)** The Cu-AHP lignin hydrogenolysis products in the flow-reactor: 1 mg/mL Cu-AHP lignin dissolved in dioxane/water (9:1, v/v), 50 mg 5% Pd/C, 800 psi H₂ (STP). The temperature of the reactor was set to 190 °C, changed to 160 °C at 220 min, and decreased to 140 °C at 360 min. **c)** GPC Chromatogram of Cu-AHP lignin and hydrogenolysis products of Cu-AHP lignin in a flow reactor at 140-190 °C and in a batch reactor at 200 °C. The x-axis is the elution time, and the y-axis is the UV absorbance at 280 nm. Monomer yields are reported in Table S4. The Mw for all lignin depolymerization products were calibrated using synthetic lignin model compounds (Fig. S37).

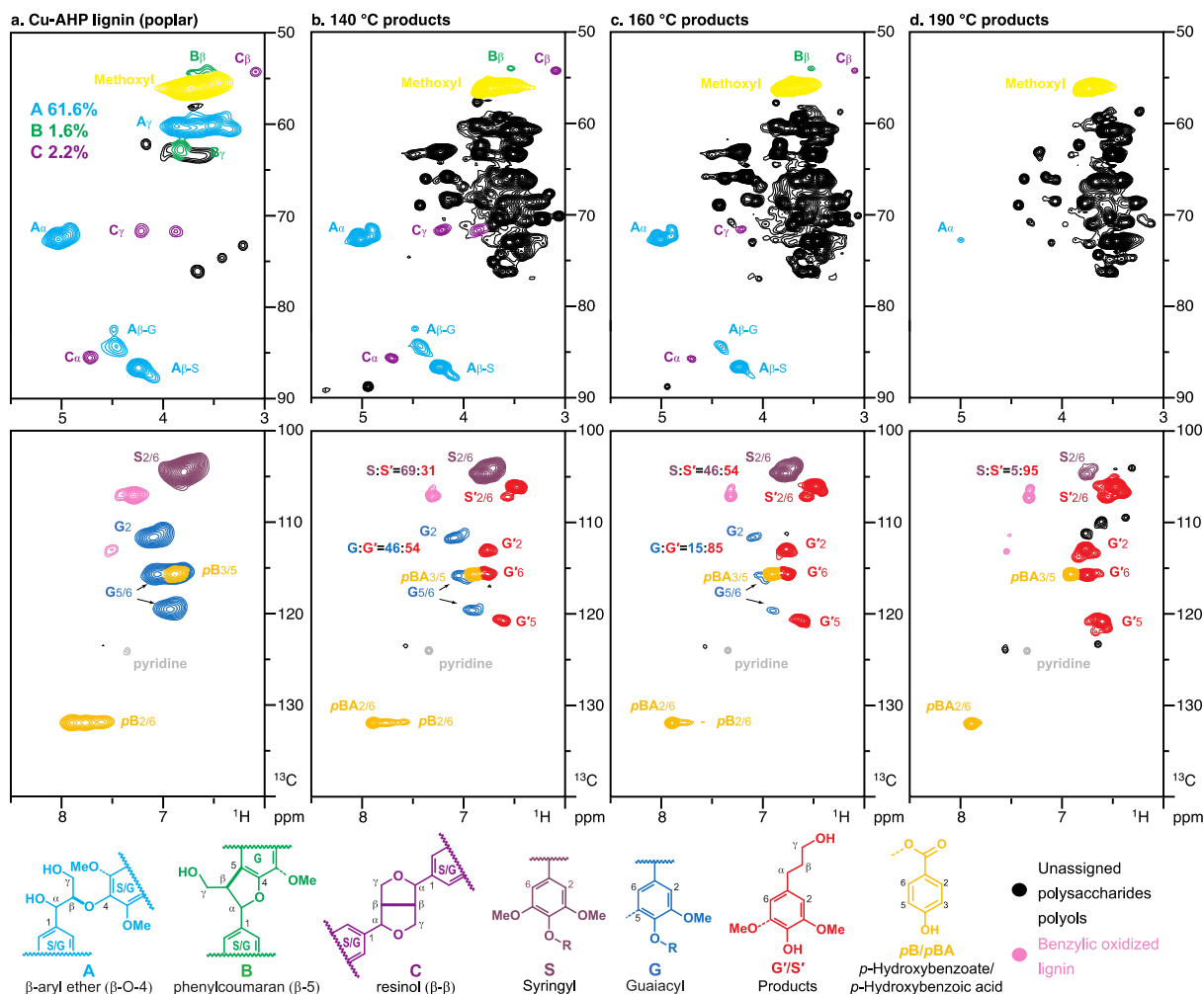


Figure 4. Partial 2D HSQC NMR spectra of a) Cu-AHP lignin obtained from poplar; Cu-AHP lignin hydrogenolysis products after flow-tube reaction: b) at 140 °C; c) at 160 °C; d) at 190 °C. The top four spectra: Lignin sidechain fingerprint region (δ_{H} 3.0-5.5 ppm, δ_{C} 50-90 ppm). The bottom four spectra: Aromatic region (δ_{H} 6.0-8.5 ppm, δ_{C} 100-140 ppm). Possible lignin oligomers are summarized in Table S4.

Table 1: Turnover frequency (TOF) and Reaction Rate Parameters for GG and VG Model Compounds. Hydrogen partial pressure varied from 500 to 900 psi. Model compound concentration varied from 1 mg/mL to 4 mg/mL. The temperature for the model compound hydrogenolysis ranged from 100 °C to 115 °C for **GG** and from 105 °C to 120 °C for **VG** under 20 mL/min H₂ flow. The temperature for the catalytic reactions of model compounds under Ar ranged from 105 °C to 125 °C for **GG** and from 120 °C to 140 °C for **VG** under 20 mL/min Ar flow. The rate of ether cleavage was calculated using the production rate of **G**.

Reactant	Rate of ether cleavage (mol/min/g)	TOF (s ⁻¹)*	k (1/M ^(m+n) /s)	Model Compound Order (m)	Hydrogen Order (n)	Activation Energy (E _a) [kJ/mol]	Pre-exponential factor (A) [1/M ^(m+n) /s]
GG	6.19E-06	1.88E-03	9.95E-02	0.73	0.16	72.16	6.85E+08
VG	2.80E-06	8.49E-04	4.50E-02	0.64	0.27	77.65	1.74E+09

*The site density of 5% Pd/C was found to be 55 μmoles of sites/g catalyst, according to CO chemisorption (Fig. S2).

References

1. A. J. Ragauskas, G. T. Beckham, M. J. Bidddy, R. Chandra, F. Chen, M. F. Davis, B. H. Davison, R. A. Dixon, P. Gilna, M. Keller, P. Langan, A. K. Naskar, J. N. Saddler, T. J. Tschaplinski, G. A. Tuskan and C. E. Wyman, *Science*, 2014, **344**, 1246843_1246841-1246810.
2. W. Schutyser, T. Renders, S. Van den Bosch, S.-F. Koelewijn, G. T. Beckham and B. F. Sels, *Chemical Society Reviews*, 2018, **47**, 852-908.
3. Z. Sun, B. Fridrich, A. de Santi, S. Elangovan and K. Barta, *Chemical Reviews*, 2018, **118**, 614-678.
4. R. Rinaldi, R. Jastrzebshi, M. T. Clough, J. Ralph, M. Kennema, P. C. A. Bruijninx and B. M. Weckhuysen, *Angewandte Chemie (International Edition)*, 2016, **55**, 8164-8215.
5. R. C. Armstrong, C. Wolfram, K. P. de Jong, R. Gross, N. S. Lewis, B. Boardman, A. J. Ragauskas, K. Ehrhardt-Martinez, G. Crabtree and M. V. Ramana, *Nature Energy*, 2016, **1**, 15020.
6. Y. Mottiar, R. Vanholme, W. Boerjan, J. Ralph and S. D. Mansfield, *Current Opinion in Biotechnology*, 2016, **37**, 190-200.
7. R. Vanholme, B. Demedts, K. Morreel, J. Ralph and W. Boerjan, *Plant Physiology*, 2010, **153**, 895-905.
8. T. Renders, S. Van den Bosch, S.-F. Koelewijn, W. Schutyser and B. Sels, *Energy & Environmental Science*, 2017, **10**, 1551-1557.
9. E. E. Harris, J. D'Ianni and H. Adkins, *Journal of the American Chemical Society*, 1938, **60**, 1467-1470.
10. X. Liu, H. Li, L.-P. Xiao, R.-C. Sun and G. Song, *Green Chemistry*, 2019, **21**, 1498-1504.
11. H. W. Ma, H. W. Li, W. J. Zhao, L. X. Li, S. J. Liu, J. X. Long and X. H. Li, *Green Chemistry*, 2019, **21**, 658-668.
12. J. Kominek, D. T. Doering, D. A. Opulente, X.-X. Shen, X. Zhou, J. DeVirgilio, A. B. Hulfachor, M. A. McGee, M. A. McGee, S. D. Karlen, C. P. Kurtzman, A. Rokas and C. T. Hittinger, *Cell*, 2019, **176**, 1356-1366.
13. M. V. Galkin and J. S. M. Samec, *ChemSusChem*, 2016, **9**, 1544-1558.
14. T. H. Parsell, B. C. Owen, I. Klein, T. M. Jarrell, C. L. Marcum, L. J. Hauptert, L. M. Amundson, H. I. Kenttamaa, F. Ribeiro, J. T. Miller and M. M. Abu-Omar, *Chemical Science*, 2013, **4**, 806-813.
15. S. Van den Bosch, W. Schutyser, S. F. Koelewijn, T. Renders, C. M. Courtin and B. F. Sels, *Chemical Communications*, 2015, **51**, 13158-13161.
16. E. M. Anderson, M. L. Stone, M. J. Hülsey, G. T. Beckham and Y. Román-Leshkov, *ACS Sustainable Chemistry & Engineering*, 2018, **6**, 7951-7959.
17. T. Renders, G. Van den Bossche, T. Vangeel, K. Van Aelst and B. Sels, *Current Opinion in Biotechnology*, 2019, **56**, 193-201.
18. A. Das, A. Rahimi, A. Ulbrich, M. Alherech, A. H. Motagamwala, A. Bhalla, L. da Costa Sousa, V. Balan, J. A. Dumesic, E. L. Hegg, B. E. Dale, J. Ralph, J. J. Coon and S. S. Stahl, *ACS Sustainable Chemistry & Engineering*, 2018, **6**, 3367-3374.
19. D. M. Alonso, S. H. Hakim, S. Zhou, W. Won, O. Hosseinaei, J. Tao, V. Garcia-Negron, A. H. Motagamwala, M. A. Mellmer, K. Huang, C. J. Houtman, N. Labbe, D. P. Harper, C. Maravelias, T. Runge and J. A. Dumesic, *Science Advances*, 2017, **3**, e1603301.
20. D. S. Argyropoulos, Y. Sun and E. Palus, *J. Pulp and Paper Sci.*, 2002, **28**, 50-54.
21. J. Ralph, C. Lapiere and W. Boerjan, *Current Opinion in Biotechnology, Special issue on Lignin Engineering*, 2019, **56**, 240-249.
22. Y. Li, L. Shuai, H. Kim, A. H. Motagamwala, J. K. Mobley, F. Yue, Y. Tobimatsu, D. Havkin-Frenkel, F. Chen, R. A. Dixon, J. S. Luterbacher, J. A. Dumesic and J. Ralph, *Science Advances*, 2018, **4**, eaau2968, 2961-2910.
23. A. Bhalla, N. Bansal, S. Pattathil, M. Li, W. Shen, C. A. Particka, R. Semaan, E. Gonzales-Vigil, S. D. Karlen, J. Ralph, S. D. Mansfield, S.-Y. Ding, D. B. Hodge and E. L. Hegg, *ACS Sustainable Chemistry & Engineering*, 2018, **6**, 2932-2941.
24. L. Shuai, M. T. Amiri, Y. M. Questell-Santiago, F. Héroguel, Y. Li, H. Kim, R. Meilan, C. Chapple, J. Ralph and J. S. Luterbacher, *Science*, 2016, **354**, 329-333.

25. W. Lan, M. Talebi Amiri, C. M. Hunston and J. S. Luterbacher, *Angewandte Chemie (International Edition)*, 2018, **57**, 1356-1360.
26. J. S. Luterbacher, A. Azarpira, A. H. Motagamwala, F. Lu, J. Ralph and J. A. Dumesic, *Energy and Environmental Science*, 2015, **8**, 2657-2663.
27. A. Sluiter, B. Hames, R. Ruiz, C. Scarlata, J. Sluiter, D. Templeton and D. Crocker, *Laboratory Analytical Procedure (LAP)-Technical Report*, 2012, NREL/TP-510-42618.
28. E. Feghali, G. Carrot, P. Thuéry, C. Genre and T. Cantat, *Energy & Environmental Science*, 2015, **8**, 2734-2743.
29. Q. Song, F. Wang, J. Cai, Y. Wang, J. Zhang, W. Yu and J. Xu, *Energy & Environmental Science*, 2013, **6**, 994-1007.
30. C. S. Lancefield, O. S. Ojo, F. Tran and N. J. Westwood, *Angewandte Chemie (International Edition)*, 2015, **54**, 258-262.
31. T. Yokoyama, *Journal of Wood Chemistry and Technology*, 2015, **35**, 27-42.
32. R. Gao, Y. Li, H. Kim, J. K. Mobley and J. Ralph, *ChemSusChem*, 2018, **11**, 2045-2050.
33. C. W. Lahive, P. J. Deuss, C. S. Lancefield, Z. H. Sun, D. B. Cordes, C. M. Young, F. Tran, A. M. Z. Slawin, J. G. de Vries, P. C. J. Kamer, N. J. Westwood and K. Barta, *Journal of the American Chemical Society*, 2016, **138**, 8900-8911.
34. A. Azarpira, J. Ralph and F. Lu, *BioEnergy Research*, 2014, **7**, 78-86.
35. F. Lu and J. Ralph, *Journal of Agricultural and Food Chemistry*, 1997, **45**, 4655-4660.
36. A. Rahimi, A. Azarpira, H. Kim, J. Ralph and S. S. Stahl, *Journal of the American Chemical Society*, 2013, **135**, 6415-6418.
37. J. F. Hartwig and A. G. Sergeev, *Science*, 2011, **332**, 439-443.
38. S. Shimizu, P. Posoknistakul, T. Akiyama, T. Yokoyama and Y. Matsumoto, *Journal of Wood Science*, 2018, 1-11.
39. X. Pan, F. Pla, D. Lachenal, C. Lapierre and B. Monties, *Journal of Wood Chemistry and Technology*, 1992, **12**, 279-298.
40. M. Dolk, J. F. Yan and J. L. McCarthy, *Holzforschung-International Journal of the Biology, Chemistry, Physics and Technology of Wood*, 1989, **43**, 91-98.
41. I. Kumaniaev, E. Subbotina, J. Sävmarker, M. Larhed, M. V. Galkin and J. S. Samec, *Green Chemistry*, 2017, **19**, 5767-5771.
42. E. M. Anderson, M. L. Stone, R. Katahira, M. Reed, G. T. Beckham and Y. Román-Leshkov, *Joule*, 2017, **1**, 613-622.
43. S. Omori, M. Aoyama and A. Sakakibara, *Holzforschung*, 1998, **52**, 391-397.
44. T. Kishimoto, A. Ueki, H. Takamori, Y. Uraki and M. Ubukata, *Holzforschung*, 2002, **56**, 623-631.
45. T. Kishimoto and Y. Sano, *Holzforschung*, 2001, **55**, 611-616.
46. W. Schutyser, S. Van den Bosch, T. Renders, T. De Boe, S. F. Koelewijn, A. Dewaele, T. Ennaert, O. Verkinderen, B. Goderis, C. M. Courtin and B. F. Sels, *Green Chemistry*, 2015, **17**, 5035-5045.
47. D. J. van de Pas, B. Nanayakkara, I. D. Suckling and K. M. Torr, *Holzforschung*, 2014, **68**, 151-155.
48. M. A. Mellmer, C. Sanpitakseree, B. Demir, P. Bai, K. W. Ma, M. Neurock and J. A. Dumesic, *Nature Catalysis*, 2018, **1**, 199-207.
49. T. W. Walker, A. K. Chew, H. X. Li, B. Demir, Z. C. Zhang, G. W. Huber, R. C. Van Lehn and J. A. Dumesic, *Energy & Environmental Science*, 2018, **11**, 617-628.
50. J. V. H. d'Angelo and A. Z. Francesconi, *Journal of Chemical and Engineering Data*, 2001, **46**, 671-674.